

# Water-Based Conductive Ink Formulations for Enzyme-Based Wearable Biosensors

Angelo Tricase, Anna Imbriano, Marlene Valentino, Nicoletta Ditaranto, Eleonora Macchia, Cinzia Di Franco, Reshma Kidayaveetil, Dónal Leech, Matteo Piscitelli, Gaetano Scamarcio, Gaetano Perchiazzi, Luisa Torsi,\* and Paolo Bollella\*

Herein, this work reports the first example of second-generation wearable biosensor arrays based on a printed electrode technology involving a water-based graphite ink, for the simultaneous detection of L-lactate and D-glucose. The water-based graphite ink is deposited onto a flexible polyethylene terephthalate sheet, namely stencil-printed graphite (SPG) electrodes, and further modified with [Os(bpy)<sub>2</sub>(Cl)(PVI)<sub>10</sub>] as an osmium redox polymer to shuttle the electrons from the redox center of lactate oxidase from *Aerococcus viridans* (LOx) and glucose oxidase from *Aspergillus niger* (GOx). The proposed biosensor array exhibits a limit of detection as low as  $(9.0 \pm 1.0) \times 10^{-6}$  M for LOx/SPG-[Os(bpy)<sub>2</sub>(Cl)(PVI)<sub>10</sub>] and  $(3.0 \pm 0.5) \times 10^{-6}$  M for GOx/SPG-[Os(bpy)<sub>2</sub>(Cl)(PVI)<sub>10</sub>], a sensitivity as high as  $1.32 \mu\text{A mM}^{-1}$  for LOx/SPG-[Os(bpy)<sub>2</sub>(Cl)(PVI)<sub>10</sub>] and  $28.4 \mu\text{A mM}^{-1}$  for GOx/SPG-[Os(bpy)<sub>2</sub>(Cl)(PVI)<sub>10</sub>]. The technology is also selective when tested in buffer and artificial sweat and is endowed with an operational/storage stability of  $\approx 80\%$  of the initial signal retained after 20 days. Finally, the proposed array is integrated in a wristband and successfully tested for the continuous monitoring of L-lactate and D-glucose in a healthy volunteer during daily activity. This is foreseen as a real-time wearable device for sport-medicine and healthcare applications.

## 1. Introduction

In the last decades, the increasing interest in developing low-cost wearable electrochemical biosensors for remote sensing pushed many researchers to look for new technological and research solutions capable to decrease manufacturing costs and enhance the reliability/reproducibility as well as stability of such biosensing platforms.<sup>[1-4]</sup> In particular, biosensors manufacturing is constantly requesting novel materials and electrode preparation techniques that could address the aforementioned issues.<sup>[5-8]</sup> Although conductive inks were reported already a few decades ago mainly to repair electrical circuits, they are still expensive and require specific curing procedures with long preparation time and high temperatures.<sup>[9,10]</sup> Besides technological issues, these inks are generally dispersed in organic solvents, which are responsible for lower

A. Tricase, M. Valentino, N. Ditaranto, L. Torsi, P. Bollella  
 Dipartimento di Chimica  
 Università degli Studi di Bari Aldo Moro  
 Bari 70125, Italy  
 E-mail: luisa.torsi@uniba.it; paolo.bollella@uniba.it

A. Tricase, A. Imbriano, N. Ditaranto, E. Macchia, L. Torsi, P. Bollella  
 Centre for Colloid and Surface Science  
 Università degli Studi di Bari Aldo Moro  
 Bari 70125, Italy

E. Macchia  
 Dipartimento di Farmacia-Scienze del Farmaco  
 Università degli Studi di Bari Aldo Moro  
 Bari 70125, Italy


E. Macchia, L. Torsi  
 Faculty of Science and Engineering  
 Åbo Akademi University  
 Turku 20500, Finland

C. D. Franco, G. Scamarcio  
 Istituto di Fotonica e Nanotecnologie CNR  
 c/o Dipartimento Interateneo di Fisica  
 Università degli Studi di Bari Aldo Moro  
 Bari 70125, Italy

R. Kidayaveetil, D. Leech  
 School of Biological and Chemical Sciences and Ryan Institute  
 University of Galway  
 University Road, Galway H91 TK33, Ireland

M. Piscitelli, G. Scamarcio  
 Dipartimento Interateneo di Fisica  
 Università degli Studi di Bari Aldo Moro  
 Bari 70125, Italy

G. Perchiazzi  
 Department of Surgical Sciences  
 Anaesthesiology and Intensive Care  
 Uppsala University  
 Akademiska sjukhuset, Ingång 70, Uppsala 751 85, Sweden

 The ORCID identification number(s) for the author(s) of this article can be found under <https://doi.org/10.1002/adsr.202300036>

© 2023 The Authors. Advanced Sensor Research published by Wiley-VCH GmbH. This is an open access article under the terms of the Creative Commons Attribution License, which permits use, distribution and reproduction in any medium, provided the original work is properly cited.

DOI: 10.1002/adsr.202300036

conductivities and poisoning of biological recognition elements (e.g., redox enzymes, antibodies, DNA, etc.).<sup>[11–13]</sup> Nowadays, the development of water-based lab-made inks triggered the possibility of building (bio)sensors architectures with electrochemical performance (e.g., electroactive area, electron transfer rate constant, etc.) comparable with solid electrodes already reported in the literature.<sup>[14–17]</sup>

To develop reliable sensor devices, the ink mixtures should exhibit homogeneous composition, with conductive characteristics and a moderate drying time.<sup>[18]</sup> Indeed, fast drying can promote cracks on the surface, being a problem for the electrode manufacturing, while slow drying hinders the process scalability as well as specific electrode shaping/sizing.<sup>[12]</sup> In addition, water-based conductive inks enabled the possibility to minimize the production of organic solvents waste achieving zero eco-impact of point-of-care biosensing market, which has been widely emphasized during COVID-19 pandemic emergency.<sup>[1,19–21]</sup>

To ensure a high level of reproducibility and robustness wearable enzyme-based biosensors needs to be tested in real operating conditions.<sup>[22,23]</sup> This requires all analyses to be performed considering the blood/tissue or peripheral bodily fluid ratio that can be affected by several factors (e.g., hormonal dysfunctions, sweating rate, age, etc.). Besides the reproducibility, the robustness is affected by the immobilization of bioreceptors.<sup>[1]</sup> In this regard, a big step forward is the possibility to print enzymes directly onto a conductive support or embedding them within a conductive ink.<sup>[24,25]</sup> The latter can be easily achieved by considering the newly developed water-based conductive inks. In addition, the roughness/porosity of such electrode surface can prevent enzyme denaturation creating a diffusion barrier that will reduce signal variation and minimize the loss of enzymatic activity.<sup>[26]</sup>

Enzyme-based biosensors rely on redox enzymes enabling the catalytic oxidation/reduction of their substrates.<sup>[27–32]</sup> Most lactate and glucose biosensors are developed considering LOx and GOx as bioreceptors, respectively. LOx contains flavin mononucleotide (FMN) catalyzing the oxidation of lactate to pyruvate with the contemporaneous reduction of O<sub>2</sub> to H<sub>2</sub>O<sub>2</sub>. Since O<sub>2</sub> is naturally working as an electron acceptor, both O<sub>2</sub> and the related product H<sub>2</sub>O<sub>2</sub> can be electrochemically monitored to obtain an amperometric output that is proportional to lactate concentration.<sup>[33,34]</sup> However, there are several concerns about the selectivity and reproducibility of the results about these first-generation lactate biosensors, mainly due to the required high overpotential needed to oxidize/reduce H<sub>2</sub>O<sub>2</sub> and the fluctuation of O<sub>2</sub> in the solution, not considering its limited availability while working in bodily fluids (0.22 × 10<sup>−3</sup> M). Similarly, GOx contains flavin adenine dinucleotide (FAD) catalyzing glucose oxidation accompanied by O<sub>2</sub> reduction to H<sub>2</sub>O<sub>2</sub>.<sup>[28,35]</sup> Despite its initial “fame” among bioelectrochemists, describing it as “ideal enzyme,” nowadays, GOx is considered a reliable biocatalyst to develop only first- and second-generation biosensors. Indeed, GOx does not undergo direct electron transfer (DET) with electrodes.<sup>[36,37]</sup>

Besides the enzymatic detection, many analytical methods have been proposed for the detection of lactate and glucose, such as chemiluminescence,<sup>[38]</sup> high-performance liquid chromatography<sup>[39]</sup> and magnetic resonance spectroscopy.<sup>[40]</sup> However, these methods have known drawbacks, as they are often time-consuming, expensive and require laboratory equip-

ment and trained personnel. Amperometric enzyme-based biosensors represent a valid approach particularly for the development of wearable biosensors for continuous metabolites monitoring and remote medicine.<sup>[20,23]</sup>

This work reports on the formulation of water-based graphite inks to fabricate stencil-printed electrodes (**Figure 1**). The water-based inks are formulated using graphite, chitosan with medium molecular weight and glycerol, as conductive material, binder, and stabilizer, respectively. The proposed ink was further reformulated including Prussian Blue (PB) to develop an active ink toward H<sub>2</sub>O<sub>2</sub> reduction to implement first-generation enzyme-based biosensors. Furthermore, the stencil-printed graphite electrode was modified with osmium redox polymers (ORPs) and LOx/GOx to develop, for the first time, an array of second-generation biosensors based on water-based conductive ink. After preliminary characterization performed in buffer and artificial sweat, the proposed array was integrated into a wrist band to continuously monitor lactate and glucose during daily activities with the results showing promise for future applications in remote personalized medicine.

## 2. Results and Discussion

### 2.1. Electrochemical, Spectroscopic, and Morphological Characterization of Stencil-Printed Graphite Electrodes

Graphite electrodes were obtained by stencil-printing on a flexible support, namely polyethylene terephthalate (PET), as specified in the experimental section. To perform a preliminary characterization, both stencil-printed graphite (SPG) electrode and a commercial screen-printed graphite electrode were analyzed by using cyclic voltammetry (CV) in 5 × 10<sup>−3</sup> M Fe(CN)<sub>6</sub><sup>3−/4−</sup>, as reported in **Figure 2A**. The SPG electrode shows a peak-to-peak separation of 0.237 V at 50 mV s<sup>−1</sup> (**Figure 2A**, red curve), which is smaller than that at the screen-printed graphite electrode (**Figure 2A**, black curve, 0.614 V). In addition, both electrodes were scanned at different scan rates (*data not shown*) to determine the electroactive area (*A*<sub>EA</sub>), roughness factor (*ρ*) and electron transfer rate constant (*k*<sup>0</sup>, cm s<sup>−1</sup>). The SPG electrode has an *A*<sub>EA</sub> of 4.11 ± 0.13 cm<sup>2</sup>, a roughness factor of 45.7 ± 1.4 (calculated by dividing the electroactive area by the geometric area) and an electron transfer rate constant of (9.7 ± 0.7) × 10<sup>−3</sup> cm s<sup>−1</sup> compared to the screen-printed graphite electrode exhibited an *A*<sub>EA</sub> of 0.89 ± 0.02 cm<sup>2</sup>, a roughness factor of 7.1 ± 0.2 and an electron transfer rate constant of (2.6 ± 0.2) × 10<sup>−4</sup> cm s<sup>−1</sup>. The electroactive area was calculated by using Randle’s–Ševčík equation.<sup>[41]</sup> The electron transfer rate constants (*k*<sup>0</sup>, cm s<sup>−1</sup>) were calculated using an extended method merging the Klingler–Kochi and Nicholson and Shain methods for totally irreversible and reversible systems.<sup>[42]</sup> In particular, the stencil-printed electrodes exhibited better electrochemical performance both in terms of electroactive area and electron transfer rate probably because of the absence of organic solvents, commonly present in commercially available inks that lead to decreased electrical conductivity, the enhanced content of graphite, reduced curing time and lower curing temperature with respect to commercial screen-printed electrodes.<sup>[12]</sup> The SPG electrodes characterized by scanning-electron microscopy (SEM) exhibit a rough surface (**Figure 2B**), confirming the high roughness factor of these electrodes. SPG electrodes were analyzed also

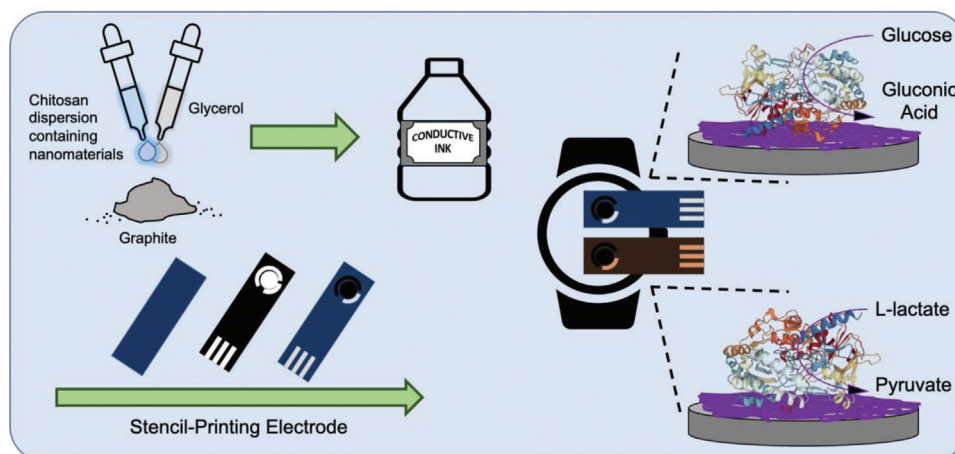


**Figure 1.** Schematic representation of water-based conductive ink formulation and further integration of stencil-printed electrodes within a wristband with second-generation lactate and glucose biosensors.

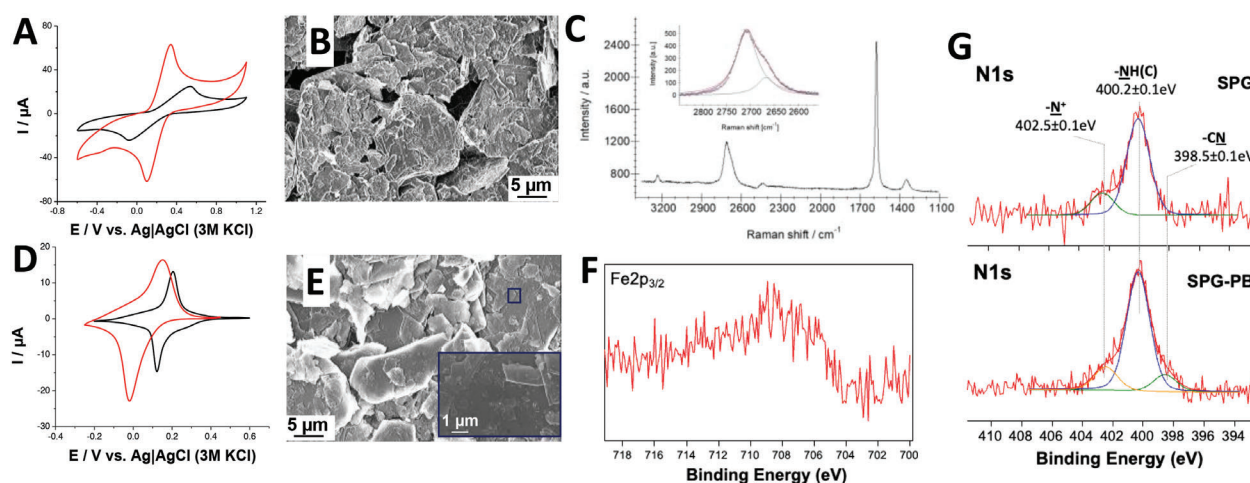


**Figure 2.** A) CVs at  $50 \text{ mV s}^{-1}$  scan rate of SPG electrode (red curve) and screen-printed graphite electrode DRP-C110 recorded in  $5 \times 10^{-3} \text{ M Fe(CN)}_6^{3-/4-}$  (prepared in  $10 \times 10^{-3} \text{ M HEPES buffer pH 7.2} + 100 \times 10^{-3} \text{ M KCl}$ ); B) SEM picture of SPG electrodes; C) Raman spectrum of SPG electrodes at  $\lambda_{\text{exc}} = 532 \text{ nm}$ ; D) CVs at  $50 \text{ mV s}^{-1}$  scan rate of SPG-PB in  $100 \times 10^{-3} \text{ M KCl pH} = 3$  (black curve) and  $10 \times 10^{-3} \text{ M HEPES buffer pH 7.2} + 100 \times 10^{-3} \text{ M KCl}$  (red curve); E) SEM picture of SPG-PB electrodes at magnification 5.00 KX—inset: SEM picture of SPG-PB electrodes; F)  $\text{Fe}2p_{3/2}$  XP spectrum relative to a typical SPG-PB electrode; G) comparison of curve-fitted N1s XP spectra relative to a typical SPG and SPG-PB electrodes.

by Raman spectroscopy, as shown in Figure 2C. Raman spectrum shows a G-band at  $1572 \text{ cm}^{-1}$ , attributed to the  $\text{sp}^2$ -type binding of carbon atoms, typical of carbon-based species. The D-band is observed at  $1348 \text{ cm}^{-1}$ , associated with the breathing mode of  $\text{sp}^2$ -carbon rings, and its second order process, the 2D band, appearing at  $2695 \text{ cm}^{-1}$ . A deeper analysis of 2D band, shown in the inset, reveals that it consists of two sub-bands, a more intense one around  $2708 \text{ cm}^{-1}$  and another at  $2667 \text{ cm}^{-1}$ , as expected for graphite.<sup>[43]</sup> Also the D' band appears around  $1618 \text{ cm}^{-1}$ , together with its first overtone at  $2336 \text{ cm}^{-1}$ . D and D' bands are related to structural disorder, being originated by scattering with defects, respectively in intervalley and intravalley processes.<sup>[44]</sup> The integrated intensity ratio  $I_D/I_G$  for the D band and G band is widely used for characterizing the defect quantity in graphitic materials. In particular, SPG electrodes showed a very low integrated intensity ratio  $I_D/I_G$  of 0.25, hence the electronic properties of graphite are not affected during the ink formulation.<sup>[45]</sup>

An active water-based ink was formulated enclosing chemically synthesized Prussian Blue (PB) nanoparticles chemically synthesized to fabricate stencil-printed electrodes, named thereafter SPG-PB electrodes. PB or ferric ferrocyanide is a well-known coordination compound with ferric ions coordinated to nitrogen and ferrous coordinated to carbon in a face centered cubic lattice.<sup>[46]</sup> Usually, PB is electrochemically deposited using a mixture of  $\text{Fe}^{3+}$  and  $[\text{Fe(CN)}_6]^{3-}$ .<sup>[47]</sup> PB nanoparticles are reported to behave as nanozymes with peroxidase-like activity.<sup>[48,49]</sup> Figure 2D displays CVs for SPG-PB electrodes at  $\text{pH} = 3$  (black curve) and  $\text{pH} = 7.2$  (red curve). The Prussian Blue/Prussian White redox activity with potassium as the counter cation is observed in both CVs as a set of sharp peaks with separation of  $80 \text{ mV}$  at  $\text{pH} = 3$  and  $168 \text{ mV}$  at  $\text{pH} = 7.2$  and  $50 \text{ mV s}^{-1}$  as scan rate. These peaks, in particular the cathodic one, are like the peaks from anodic demetallization.<sup>[50]</sup> Such set of sharp peaks in CVs correspond to the regular structure of PB with homogeneous

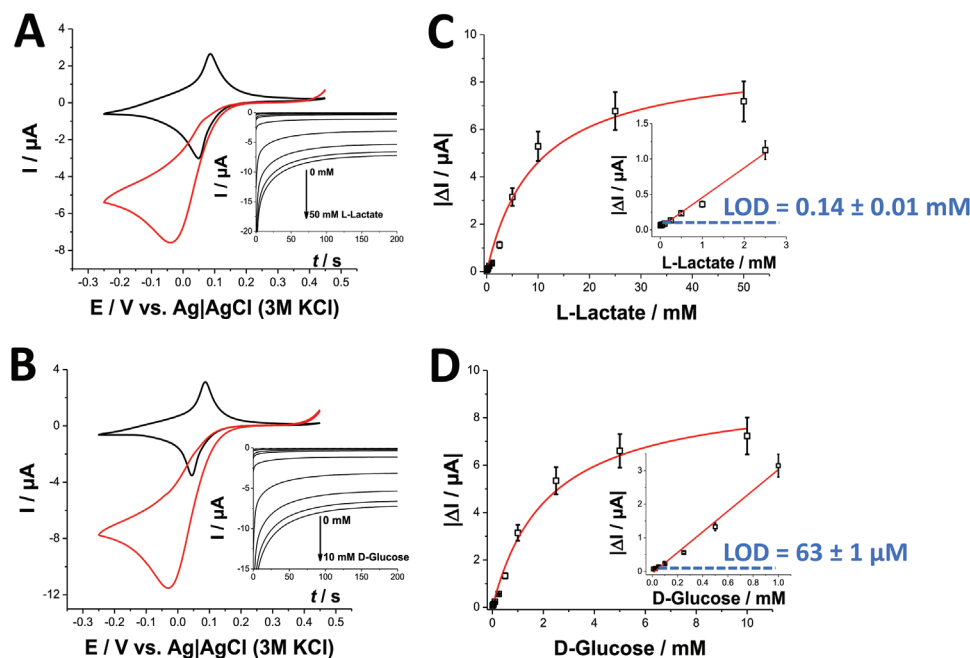


**Figure 3.** A) CVs for LOx/SPG-PB electrode in non-turnover ( $10 \times 10^{-3}$  M buffer pH = 7.2 +  $100 \times 10^{-3}$  M KCl, black curve) and turnover conditions (addition of  $10 \times 10^{-3}$  M L-lactate, red curve), scan rate  $5 \text{ mV s}^{-1}$ —inset: amperometry at  $E_{\text{appl}}: -0.1 \text{ V}$  by increasing substrate concentration in the range  $(0-5) \times 10^{-3}$  M for L-lactate; B) CVs for GOx/SPG-PB electrode in non-turnover ( $10 \times 10^{-3}$  M buffer pH = 7.2 +  $100 \times 10^{-3}$  M KCl, black curve) and turnover conditions (addition of  $10 \times 10^{-3}$  M D-glucose, red curve), scan rate  $5 \text{ mV s}^{-1}$ —inset: amperometry at  $E_{\text{appl}}: -0.1 \text{ V}$  by increasing substrate concentration in the range  $(0-10) \times 10^{-3}$  M for D-glucose; C) calibration curve for LOx/SPG-PB electrode in  $10 \times 10^{-3}$  M buffer pH = 7.2 +  $100 \times 10^{-3}$  M KCl based on the amperometric measurements performed at  $E_{\text{appl}}: -0.1 \text{ V}$  by increasing substrate concentration in the range  $(0-50) \times 10^{-3}$  M for L-lactate—inset: linear range of calibration curve for GOx/SPG-PB; D) calibration curve for GOx/SPG-PB electrode in  $10 \times 10^{-3}$  M buffer pH = 7.2 +  $100 \times 10^{-3}$  M KCl based on the amperometric measurements performed at  $E_{\text{appl}}: -0.1 \text{ V}$  by increasing substrate concentration in the range  $(0-10) \times 10^{-3}$  M for D-glucose—inset: linear range of calibration curve for GOx/SPG-PB.

distribution of charge and ion transfer rates throughout the film. To confirm the presence of PB nanoparticles, SPG-PB electrodes were analyzed by SEM, as shown in Figure 2E, displaying the rough graphite surface decorated with PB nanoparticles with diameter ranging from 20 to 100 nm (Figure 2E, inset). PB nanoparticles are well dispersed in the ink, not agglomerated as normally occurring for drop-casting deposition limiting availability for catalytic reactions on the superficial layer of the electrode.

The surface chemical composition analysis of the electrodes was performed by using XPS to investigate the presence on the surface of PB nanoparticles. From the wide scan XP spectrum it was possible to observe the presence of Fe and N, whose high resolution spectral regions are shown in Figure 2F,G. Moreover, to discriminate nitrogen coming from PB nanoparticles from nitrogen of chitosan, the curve fitting procedure was applied to N 1s XP spectra and the  $-\text{CN}$  peak component at  $\text{BE} = 398.5 \pm 0.1 \text{ eV}$  was identified in SPG-PB spectrum (Figure 2G).

## 2.2. First-Generation Lactate and Glucose Biosensors with Stencil-Printed Graphite Electrodes

The so-prepared SPG-PB electrodes were further modified with lactate oxidase (LOx) and glucose oxidase (GOx) to develop first-generation lactate and glucose biosensors, respectively. Figure 3A shows the CVs in non-turnover (black curve) and turnover conditions (addition of  $10 \times 10^{-3}$  M L-lactate, red curve). In non-

turnover conditions, SPG-PB electrodes showed reversible peaks at  $E^0 = 0.067 \text{ V}$  related to the PB nanoparticles enclosed in the water-based ink (Figure 3A, black curve). After substrate addition, a significant, mass-transfer limited, electrocatalytic curve starting at  $E_{\text{ONSET}} = 0.145 \text{ V}$  with maximum current of  $-7.6 \mu\text{A}$  at  $E = -0.040 \text{ V}$  (Figure 3A, red curve) was observed. Similarly, SPG-PB electrodes were modified with GOx showing a CV with reversible peaks at  $E^0 = 0.067 \text{ V}$  related to the PB active ink (Figure 3B, black curve). After substrate addition, an electrocatalytic curve starting at  $E_{\text{ONSET}} = 0.194 \text{ V}$  with maximum current of  $-11.5 \mu\text{A}$  at  $E = -0.030 \text{ V}$  (Figure 3B, red curve) was observed. In both cases the mass-transfer limitation is related to the nanostructured PB film, which enhances catalytic efficiency toward  $\text{H}_2\text{O}_2$  reduction, and high roughness/porosity of SPG electrodes, responsible for controlling the diffusion at the electrode surface.

The modified electrodes were tested in amperometry by increasing substrate concentration in the range  $(0-50) \times 10^{-3}$  M for L-lactate (Figure 3A, inset) and  $(0-10) \times 10^{-3}$  M for D-glucose (Figure 3B, inset), respectively.

The calibration curve from the amperometric response for LOx/SPG-PB electrodes (spanning overall the  $1 \times 10^{-6}$  to  $5 \times 10^{-2}$  M), reported in Figure 3C, indicated a linear range from  $0.45 \times 10^{-3}$  to  $2.5 \times 10^{-3}$  M (Figure 3C, inset), a detection limit (LOD) of  $(0.14 \pm 0.01) \times 10^{-3}$  M (calculated as  $\text{LOD} = 3.3 \times (\sigma/S)$  where  $\sigma$  is the absolute standard deviation of the intercept, and  $S$  is the slope of the calibration curve) and a sensitivity of  $0.41 \mu\text{A mM}^{-1}$  with a correlation coefficient of 0.98 (RSD 6.5%,  $n = 10$ ).

Additionally, the calibration curve was fitted to determine the classical Michaelis–Menten kinetic parameters, which resulted in  $I_{\max}$  of  $9.2 \pm 0.4 \mu\text{A}$  and an apparent Michaelis–Menten constant ( $K_M^{\text{app}}$ ) of  $(9.7 \pm 1.2) \times 10^{-3} \text{ M}$  ( $\approx 20$  times higher than  $K_M$  measured in solution).<sup>[51]</sup> The latter could be related to the controlled diffusion of enzymatic product (i.e.,  $\text{H}_2\text{O}_2$ ) through the rough electrode surface. This usually results in an extended linear range, but the dispersion of PB nanoparticles into the ink may have hindered their availability for superficial catalytic reactions, where the enzyme is physisorbed. The calibration curve for GOx/SPG-PB electrodes (spanning overall the  $1 \times 10^{-6}$  to  $1 \times 10^{-2} \text{ M}$ ), reported in Figure 3D, indicated a linear range from  $0.2 \times 10^{-3}$  to  $1 \times 10^{-3} \text{ M}$  (Figure 3D, inset), a detection limit of  $(63 \pm 1) \times 10^{-6} \text{ M}$  and sensitivity of  $3.2 \mu\text{A mm}^{-1}$  and a correlation coefficient of 0.99 (RSD 4.8%,  $n = 10$ ). The kinetic parameters were determined as  $I_{\max}$  of  $9.3 \pm 0.1 \mu\text{A}$  and a  $K_M^{\text{app}}$  of  $(2.2 \pm 0.3) \times 10^{-3} \text{ M}$  (similar to  $K_M$  measured in solution).<sup>[52]</sup> However, the reported LOD values are higher than the values reported in the literature.<sup>[53–64]</sup> Indeed, the linear ranges were narrower and the sensitivities lower than the ones previously reported.<sup>[53–64]</sup> The analytical figures of merit for both biosensors are summarized in Table S1 (Supporting Information). The analytical performance for the proposed electrode platform could be ascribed to the low amount of enzyme effectively immobilized onto the electrode surface and the superficial unavailability of PB nanoparticles toward catalytic  $\text{H}_2\text{O}_2$  reduction.

### 2.3. Second-Generation Lactate and Glucose Biosensors with Stencil-Printed Graphite Electrodes

Despite the analytical performance of first-generation biosensors, SPG electrodes were further modified by drop-casting of osmium redox polymers (ORPs),  $[\text{Os}(\text{bpy})_2(\text{Cl})(\text{PVI})_{10}]$  and  $[\text{Os}(\text{dmbpy})_2(\text{Cl})(\text{PVI})_{10}]$ , to develop second-generation lactate and glucose biosensors, still based on LOx and GOx as enzymatic bioreceptors.

Figure 4A shows the CVs in the absence (black curve) and presence of  $10 \times 10^{-3} \text{ M}$  L-lactate (red curve). In non-turnover conditions, SPG- $[\text{Os}(\text{bpy})_2(\text{Cl})(\text{PVI})_{10}]$  electrodes showed a couple of quasireversible peaks at  $E^0 = 0.205 \text{ V}$  related to LOx-modified ORP electrode (Figure 4A, black curve). After substrate addition, a catalytic curve starting at  $E_{\text{ONSET}} = 0.050 \text{ V}$  with maximum current of  $23 \mu\text{A}$  at  $E = 0.350 \text{ V}$  (Figure 4A, red curve) was observed. Similarly, SPG- $[\text{Os}(\text{bpy})_2(\text{Cl})(\text{PVI})_{10}]$  electrodes were modified with GOx and the corresponding CV in non-turnover conditions displayed a couple of peaks at  $E^0 = 0.250 \text{ V}$  related to GOx-modified ORP electrode (Figure 4B, black curve). After substrate addition, the catalysis for D-glucose oxidation started at  $E_{\text{ONSET}} = -0.020 \text{ V}$  with maximum current of  $35 \mu\text{A}$  at  $E = 0.390 \text{ V}$  (Figure 4B, red curve). In both cases, the mass-transfer limitation is related to high roughness/porosity of SPG electrodes, which allows to control the diffusion at the electrode surface. Afterward, LOx and GOx were drop-cast also onto  $[\text{Os}(\text{dmbpy})_2(\text{Cl})(\text{PVI})_{10}]$  modified SPG electrodes. CVs for SPG- $[\text{Os}(\text{dmbpy})_2(\text{Cl})(\text{PVI})_{10}]$  in the absence and presence of substrates are reported in Figure S1A,B (Supporting Information), displaying lower catalytic waves than SPG- $[\text{Os}(\text{bpy})_2(\text{Cl})(\text{PVI})_{10}]$  modified electrodes, maximum current of  $17.5 \pm 0.3 \mu\text{A}$  at  $E = 0.26 \text{ V}$  and  $28 \pm 1.2 \mu\text{A}$  at

$E = 0.25 \text{ V}$ . This smaller catalytic current may be due to a lower difference in thermodynamic potential between the formal potential of the  $[\text{Os}(\text{dmbpy})_2(\text{Cl})(\text{PVI})_{10}]$  ORP and the redox potential of the prosthetic group within the enzymes compared to the  $[\text{Os}(\text{bpy})_2(\text{Cl})(\text{PVI})_{10}]$  ORP.

The influence of  $\text{O}_2$  on the electrocatalytic behavior of GOx modified SPG- $[\text{Os}(\text{bpy})_2(\text{Cl})(\text{PVI})_{10}]$  electrode was tested after purging the solution with  $\text{N}_2$ . CVs in the absence (Figure S2, Supporting Information, black curve) and presence of  $10 \times 10^{-3} \text{ M}$  D-glucose (Figure S2, Supporting Information, red curve) showed a similar catalytic wave to the ones recorded in the presence of  $\text{O}_2$ , with a maximum current of  $38 \pm 2.1 \mu\text{A}$  at  $E = 0.390 \text{ V}$ .

Both modified electrodes were tested in amperometry by increasing substrate concentration in the range  $0\text{--}50 \times 10^{-3} \text{ M}$  for L-lactate (Figure 4C, inset) and  $(0\text{--}10) \times 10^{-3} \text{ M}$  for D-glucose (Figure 4D, inset), respectively.

The calibration curve for LOx/SPG- $[\text{Os}(\text{bpy})_2(\text{Cl})(\text{PVI})_{10}]$  electrodes (spanning overall the  $1 \times 10^{-6}$  to  $5 \times 10^{-2} \text{ M}$ ), reported in Figure 4C, indicated a linear range from  $30 \times 10^{-6}$  to  $5 \times 10^{-3} \text{ M}$  (Figure 4C, inset), a detection limit of  $(9 \pm 1) \times 10^{-6} \text{ M}$  and a sensitivity of  $1.32 \mu\text{A mm}^{-1}$  and a correlation coefficient of 0.97 (RSD 6.1%,  $n = 10$ ). Additionally, the calibration curve was fitted to determine the classical Michaelis–Menten kinetic parameters, which resulted in  $I_{\max}$  of  $14.8 \pm 0.6 \mu\text{A}$  and an apparent Michaelis–Menten constant ( $K_M^{\text{app}}$ ) of  $(7.8 \pm 1.1) \times 10^{-3} \text{ M}$  ( $\approx 14$  times higher than  $K_M$  measured in solution). Being both the ORP and LOx immobilized onto the surface of a rough graphite electrode,  $K_M^{\text{app}}$  values could be affected by the controlled diffusion of the enzymatic substrate. The calibration curve for GOx/SPG- $[\text{Os}(\text{bpy})_2(\text{Cl})(\text{PVI})_{10}]$  electrodes reported in Figure 4D (spanning overall the  $1 \times 10^{-6}$  to  $1 \times 10^{-2} \text{ M}$ ), indicated a linear range from  $10 \times 10^{-6}$  to  $250 \times 10^{-6} \text{ M}$  (Figure 4D, inset), a detection limit of  $(3.0 \pm 0.5) \times 10^{-6} \text{ M}$  and sensitivity of  $28.4 \mu\text{A mm}^{-1}$  and a correlation coefficient of 0.98 (RSD 5.7%,  $n = 10$ ). The kinetic parameters were determined as  $I_{\max}$  of  $19.4 \pm 0.8 \mu\text{A}$  and a  $K_M^{\text{app}}$  of  $(0.38 \pm 0.06) \times 10^{-3} \text{ M}$  (like  $K_M$  measured in solution)<sup>[52]</sup> probably related to the amount of ORP and GOx immobilized onto the electrode.

Besides the preliminary analytical features, the storage stability of the proposed platforms was tested by recording the amperometric response for 20 consecutive measurements every day over a period of 20 days. The stability measurements were performed by continuously supplying  $0.2 \times 10^{-3} \text{ M}$  L-lactate (Figure 4E, red curve) and  $0.2 \times 10^{-3} \text{ M}$  D-glucose (Figure 4E, black curve) through a FIA system. In particular, LOx/SPG- $[\text{Os}(\text{bpy})_2(\text{Cl})(\text{PVI})_{10}]$  reported a response decrease of its initial signal of 21% after 20 days, probably because of the enzyme intrinsic stability and the porosity/roughness of SPG electrodes, which is stabilizing the enzymatic layer. GOx/SPG- $[\text{Os}(\text{bpy})_2(\text{Cl})(\text{PVI})_{10}]$  showed similar storage stability trend. Furthermore, the stability of both biosensors, namely LOx/SPG- $[\text{Os}(\text{bpy})_2(\text{Cl})(\text{PVI})_{10}]$  and GOx/SPG- $[\text{Os}(\text{bpy})_2(\text{Cl})(\text{PVI})_{10}]$ , was tested by spiking artificial sweat with  $10 \times 10^{-3} \text{ M}$  L-lactate (Figure 4F, red curve) and  $10 \times 10^{-3} \text{ M}$  D-glucose (Figure 4F, black curve). Both electrode platforms, showed a stable amperometric response after substrate addition over 15 h (measurements performed with a flow-injection system to continuously provide a flow of both substrates to the electrochemical cell). The selectivity of the proposed biosensing platforms was evaluated

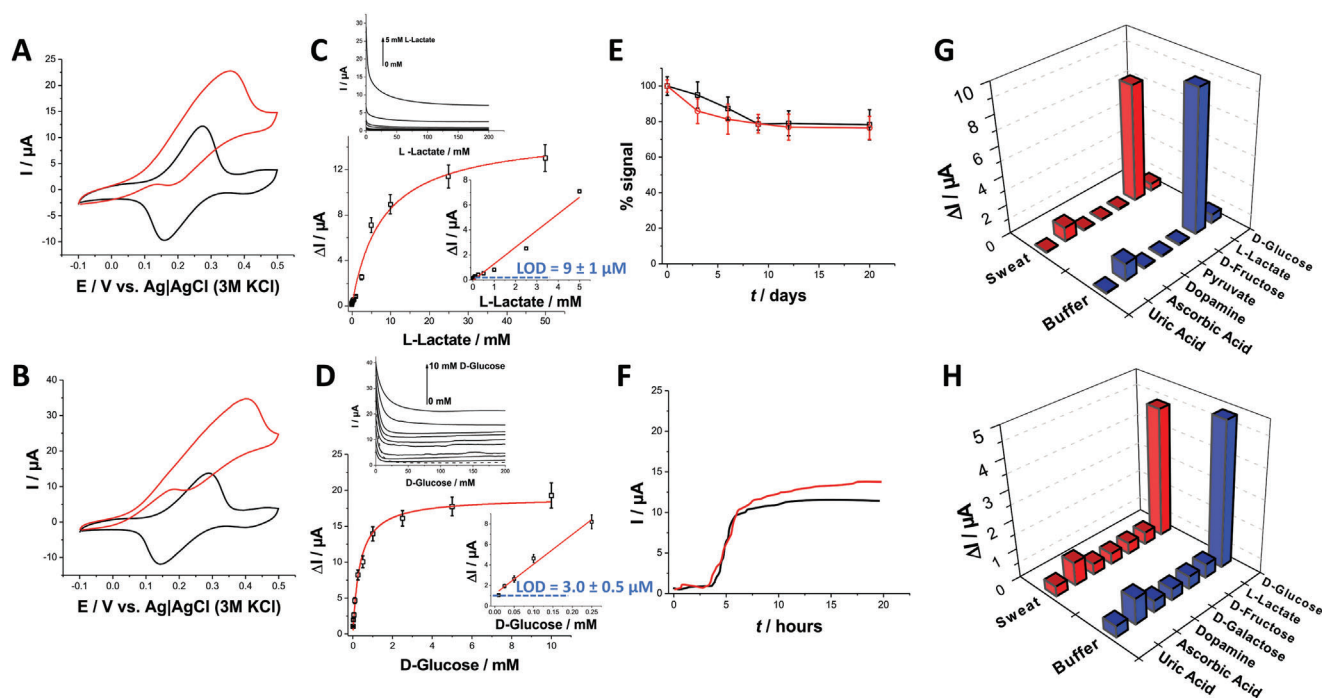


**Figure 4.** A) CVs for LOx/SPG-[Os(bpy)<sub>2</sub>(Cl)(PVI)<sub>10</sub>] electrode in non-turnover ( $10 \times 10^{-3}$  M buffer pH = 7.2 +  $100 \times 10^{-3}$  M KCl, black curve) and turnover conditions (addition of  $10 \times 10^{-3}$  M L-lactate, red curve), scan rate  $5 \text{ mV s}^{-1}$ ; B) CVs for GOx/SPG-[Os(bpy)<sub>2</sub>(Cl)(PVI)<sub>10</sub>] electrode in non-turnover ( $10 \times 10^{-3}$  M buffer pH = 7.2 +  $100 \times 10^{-3}$  M KCl, black curve) and turnover conditions (addition of  $10 \times 10^{-3}$  M D-glucose, red curve), scan rate  $5 \text{ mV s}^{-1}$ ; C) calibration curve for LOx/SPG-[Os(bpy)<sub>2</sub>(Cl)(PVI)<sub>10</sub>] electrode in  $10 \times 10^{-3}$  M buffer pH = 7.2 +  $100 \times 10^{-3}$  M KCl based on the amperometric measurements performed at  $E_{\text{app}}$ : +0.3 V by increasing substrate concentration in the range  $0\text{--}50 \times 10^{-3}$  M for L-lactate—inset 1: amperometry at  $E_{\text{app}}$ : +0.3 V by increasing substrate concentration in the range  $(0\text{--}5) \times 10^{-3}$  M for L-lactate—inset 2: linear range of calibration curve for LOx/SPG-[Os(bpy)<sub>2</sub>(Cl)(PVI)<sub>10</sub>]; D) calibration curve for GOx/SPG-[Os(bpy)<sub>2</sub>(Cl)(PVI)<sub>10</sub>] electrode in  $10 \times 10^{-3}$  M buffer pH = 7.2 +  $100 \times 10^{-3}$  M KCl based on the amperometric measurements performed at  $E_{\text{app}}$ : +0.3 V by increasing substrate concentration in the range  $(0\text{--}10) \times 10^{-3}$  M for D-glucose—inset 1: amperometry at  $E_{\text{app}}$ : +0.3 V by increasing substrate concentration in the range  $(0\text{--}10) \times 10^{-3}$  M for D-glucose; inset 2: linear range of calibration curve for GOx/SPG-[Os(bpy)<sub>2</sub>(Cl)(PVI)<sub>10</sub>]; E) stability measurements carried out over a period of 20 days for LOx/SPG-[Os(bpy)<sub>2</sub>(Cl)(PVI)<sub>10</sub>] and GOx/SPG-[Os(bpy)<sub>2</sub>(Cl)(PVI)<sub>10</sub>] by injecting  $0.2 \times 10^{-3}$  M L-lactate (red curve) and  $0.2 \times 10^{-3}$  M D-glucose (black curve). F) Operational stability measurements carried out over a period of 20 h for LOx/SPG-[Os(bpy)<sub>2</sub>(Cl)(PVI)<sub>10</sub>] and GOx/SPG-[Os(bpy)<sub>2</sub>(Cl)(PVI)<sub>10</sub>] by spiking artificial sweat with  $10 \times 10^{-3}$  M L-lactate (red curve) and  $10 \times 10^{-3}$  M D-glucose (black curve) measured with amperometry at  $E_{\text{app}}$ : +0.3 V; G) influence of interfering compounds on lactate response:  $50 \times 10^{-6}$  M ascorbic acid,  $50 \times 10^{-6}$  M uric acid,  $50 \times 10^{-6}$  M D-glucose,  $50 \times 10^{-6}$  M pyruvate,  $50 \times 10^{-6}$  M D-fructose, and  $50 \times 10^{-6}$  M dopamine and  $10 \times 10^{-3}$  M L-lactate measured with amperometry at  $E_{\text{app}}$ : +0.3 V; H) influence of interfering compounds on lactate response:  $50 \times 10^{-6}$  M ascorbic acid,  $50 \times 10^{-6}$  M uric acid,  $50 \times 10^{-6}$  M L-lactate,  $50 \times 10^{-6}$  M D-galactose,  $50 \times 10^{-6}$  M D-fructose,  $50 \times 10^{-6}$  M dopamine, and  $10 \times 10^{-3}$  M D-glucose measured with amperometry at  $E_{\text{app}}$ : +0.3 V.

toward potential interferents. The signals recorded at fixed concentration of L-lactate and D-glucose were compared with those obtained at the same concentrations of different interferents (considering their presence in human plasma),<sup>[65]</sup> both in buffer and artificial sweat. The interferents tested were D-glucose, D-fructose, pyruvate, dopamine, ascorbic and uric acid for L-lactate detection (Figure 4H), while L-lactate, D-fructose, D-galactose, dopamine, ascorbic and uric acid for D-glucose detection (Figure 4H). No significant current responses were recorded except for ascorbic acid, notably 12% of L-lactate signal and 19% of D-glucose signal, respectively. Ascorbic acid, differently from other electrochemical interferents tested exhibits higher diffusion coefficient ( $D = 5.9 \times 10^{-6} \text{ cm}^2 \text{ s}^{-1}$ ) and can be easily oxidized at the electrode surface (i.e., dopamine  $D = 8.2 \times 10^{-7} \text{ cm}^2 \text{ s}^{-1}$ ) at the potential where the analytical measurements are performed. The analytical figures of merit for both biosensor platforms are summarized in Table S2 (Supporting Information). However, LOx/SPG-[Os(bpy)<sub>2</sub>(Cl)(PVI)<sub>10</sub>] and GOx/SPG-

[Os(bpy)<sub>2</sub>(Cl)(PVI)<sub>10</sub>] exhibited analytical features, like LOD, sensitivity, linear range and storage stability that are comparable with other platforms based on classical solid-state electrodes, as reported in Table S3 (Supporting Information).<sup>[53–64]</sup>

#### 2.4. L-Lactate and D-Glucose Integrated in a Wrist Band

After preliminary analytical characterization of both first and second-generation electrodes, they were integrated within a wristband to perform continuous L-lactate and D-glucose monitoring in sweat. As shown in Figure 5A, both working electrodes, namely LOx and GOx modified, are placed within the rubber wrist band together with a printed silver pseudo-reference and a carbon-based counter electrode. The recess within the rubber wristband created an electrochemical cell with a thickness of 2 mm, which enabled sweat accumulation. The wrist band was worn by a voluntary healthy male patient.

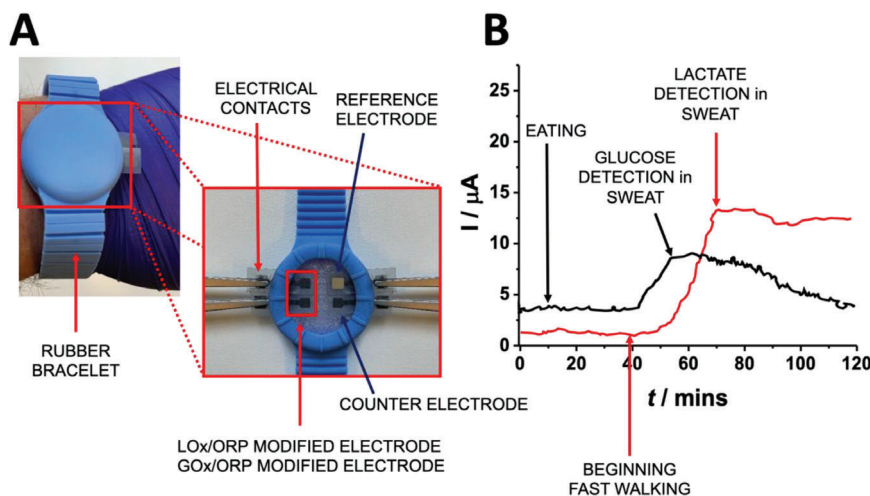


**Figure 5.** A) LOx/GOx biosensing array integrated in the wrist band with two working electrodes, a pseudo-reference and a graphite counter electrodes; B) amperometric measurements as continuous monitoring for L-lactate and D-glucose after simulating daily activities like glucose intake and lactate production during sport activity.

**Table 1.** Comparison with other biosensor arrays for lactate and glucose detection reported in literature.

Electrode platform	Bodily fluid	Linear range [ $\times 10^{-3}$ M]	Sensitivity	Generation	Ref.
GOx/Chit/MWCNTs/PB/AuE GOx/Chit/MWCNTs/PB/AuE	Sweat	0–0.2 2–30	2.35 nA $\mu\text{M}^{-1}$ 220 nA $\text{mM}^{-1}$	I	[66]
GOx/PolyHEMA/PtE LOx/PolyHEMA/PtE	Horse Serum	0–15 0–30	0.27 nA $\text{mM}^{-1}$ 0.36 nA $\text{mM}^{-1}$	I	[67]
GOx/PVP-Os-AA/MUA/AuE LOx/PVP-Os-AA/MUA/AuE	–	0–20 0–10	0.26 $\mu\text{A cm}^{-2} \text{mM}^{-1}$ 0.24 $\mu\text{A cm}^{-2} \text{mM}^{-1}$	II	[68]
GDH/pMB/ Au-MWCNTs/ AuE LOx/pMB/ Au-MWCNTs/ AuE	ISF	0.05–5 0.01–1	405.2 $\mu\text{A cm}^{-2} \text{mM}^{-1}$ 792.4 $\mu\text{A cm}^{-2} \text{mM}^{-1}$	II	[69]
GOx/SPG-[Os(bpy) <sub>2</sub> (Cl)(PVI) <sub>10</sub> ] LOx/SPG-[Os(bpy) <sub>2</sub> (Cl)(PVI) <sub>10</sub> ]	Sweat	0.1–0.25 0.03–5	315.6 $\mu\text{A cm}^{-2} \text{mM}^{-1}$ 14.7 $\mu\text{A cm}^{-2} \text{mM}^{-1}$	II	This work

Figure 5B shows the amperometric recording for L-lactate detection (red curve) during the resting state, which corresponds to  $0.2 \times 10^{-3}$  M L-lactate according to calibration curve previously measured. The amperometric signal increased to  $12.9 \mu\text{A}$  after 30 min of fast walking activity, which is in good agreement with other on-line continuous L-lactate measurements performed with previously reported wearable biosensors. Additionally, the amperometric recording for D-glucose (black curve) reported during the fasting state ( $0.06 \times 10^{-3}$  M D-glucose in sweat) accurately reflected blood physiological levels normally reported. During glucose tolerance test (drinking 200 mL D-glucose solution containing 75 grams) there was a sharp increase in the output response up to  $8.2 \mu\text{A}$ , which corresponds to  $0.23 \times 10^{-3}$  M according to the calibration curve previously measured. The latter is in good agreement with values reported for other wearable biosensors. Thereafter, the amperometric recording for D-glucose detection (black curve) decreased to the physiological level within 80 min confirming the absence of type-2 diabetes for this individual patient.

Table 1 summarizes the results obtained for other wearable or minimally invasive platforms simultaneously detecting L-lactate

and D-glucose.<sup>[66–69]</sup> The reported results account for different physiological and altered levels in a range of bodily fluids (e.g., interstitial fluid, blood, saliva, sweat, etc.). In this regard, it should be also considered the variability in terms of composition for peripheral bodily fluids, particularly for electrolytes that may affect the reproducibility of amperometric detection in sweat.

### 3. Conclusions

In this study the first example of second-generation wearable biosensor developed on water-based ink graphite electrodes for the simultaneous detection of L-lactate and D-glucose was demonstrated. The water-based graphite ink electrodes were characterized by means of cyclic voltammetry, Raman spectroscopy, XPS, and SEM. SPG-PB electrodes, containing Prussian Blue nanoparticles, were produced as first-generation biosensors, which exhibited poor analytical figures of merit with respect to developing wearable biosensors (considering the limited range for the detection of both analytes). Therefore, the water-based graphite ink, deposited onto flexible PET sheet, was further modified with [Os(bpy)<sub>2</sub>(Cl)(PVI)<sub>10</sub>] as osmium redox

polymer (ORP) to shuttle the electrons from redox center of LOx and GOx to the SPG. This biosensor array exhibited high sensitivity (notably  $1.32 \mu\text{A mm}^{-1}$  for LOx/SPG-[Os(bpy)<sub>2</sub>(Cl)(PVI)<sub>10</sub>] and  $28.4 \mu\text{A mm}^{-1}$  for GOx/SPG-[Os(bpy)<sub>2</sub>(Cl)(PVI)<sub>10</sub>]), selectivity (tested in buffer and artificial sweat) and operational/storage stability ( $\approx 80\%$  of initial signal retained after 20 days). Finally, the proposed array was integrated in a wristband and successfully tested for the continuous monitoring of L-lactate and D-glucose.

The proposed system shows promising features for deployment as a flexible and wearable biosensor based on biocompatible water-based inks which can be implemented for sport medicine and remote clinical care, possibly evolving toward edible biosensors for continuous metabolites monitoring.

## 4. Experimental Section

**Chemicals and Reagents:** 4-(2-Hydroxyethyl)piperazine-1-ethanesulfonic acid (HEPES), acetic acid (CH<sub>3</sub>COOH), D-glucose, L-lactic acid, potassium chloride (KCl), iron(III) chloride (FeCl<sub>3</sub>), potassium ferricyanide (K<sub>3</sub>Fe(CN)<sub>6</sub>), potassium ferrocyanide (K<sub>4</sub>Fe(CN)<sub>6</sub>), hydrochloric acid (HCl), sodium hydroxide (NaOH), uric acid, ascorbic acid, pyruvate, D-galactose, D-fructose, dopamine hydrochloride, isopropyl alcohol (IPA), graphite powder (<20 μm, synthetic), chitosan medium molecular weight, glycerol (ACS grade  $\geq 99.5\%$ ) and glucose oxidase (GOx) from *Aspergillus niger* were purchased from Merck Millipore (formerly Sigma Aldrich).

Lactate oxidase (LOx) from *Aerococcus viridans* was obtained from Toyobo Enzymes. The LOx (activity 300 U mL<sup>-1</sup>) was dissolved in a phosphate buffer at pH 7.4. GOx (activity 300 U mL<sup>-1</sup>) was dissolved in a phosphate buffer at pH 7.4.

Artificial human sweat or perspiration solution was provided by LCTech (Obertaufkirchen, Germany) and used without any further pretreatments.

Osmium redox polymers (ORP), namely [Os(2,2'-bipyridine)<sub>2</sub>(polyvinylimidazole)<sub>10</sub>Cl]<sup>2+/+</sup> (labeled as [Os(bpy)<sub>2</sub>(Cl)(PVI)<sub>10</sub>]) and [Os(4,4'-dimethyl-2,2'-bipyridine)<sub>2</sub>(polyvinylimidazole)<sub>10</sub>Cl]<sup>2+/+</sup> (labeled as [Os(dmbpy)<sub>2</sub>(Cl)(PVI)<sub>10</sub>]), were synthesized as previously reported.<sup>[70]</sup>

All solutions were prepared using Milli-Q water (18.2 MΩ cm, Millipore, Bedford, MA, USA).

**Water-Based Conductive Ink Formulation, Electrode Preparation, and Modification:** The water-based ink was formulated based on graphite, chitosan and glycerol as conductive material, binder, and stabilizer, respectively. A 2.5% w/v chitosan solution was prepared by dissolving chitosan into 1 M acetic acid. The latter was left under stirring at room temperature overnight. Afterward, chitosan solution was diluted at 1% w/v with distilled water (final concentration of acetic acid 0.4 M). The conductive ink was formulated by mixing 5 grams of graphite powder with 10 mL of previously prepared chitosan solution and 500 μL of glycerol.

Afterward, the SPG electrodes were prepared by using PET sheets cleaned three times with IPA and distilled water and sanded by using fine emery paper (1500 grit) to increase ink adhesion. A stencil was prepared on Smart Vinyl adhesive sheet detailly carved by using Cricut Explore 3 equipped with Design Space Software v.7.3.95. After applying the stencil on the PET sheet, 500 μL of were placed onto the PET sheet and spread with a scrape. The prepared electrode was left to dry at ambient conditions for 10 min. and cured in an oven for 1 min. at 100 °C. Later, the stencil was peeled off and the connecting track between the working electrode and the pad was insulated with nail polishing. The printed silver pseudo-reference used for the wrist band test was realized by using LOCTITE ECI 1010 E&C silver ink and cured according to manufacturing instructions.

**First-Generation LOx and GOx Electrode Preparation:** PB nanoparticles were synthesized according to previously reported methods.<sup>[71]</sup> In particular,  $2 \times 10^{-3}$  M K<sub>4</sub>Fe(CN)<sub>6</sub> was solubilized in a  $10 \times 10^{-3}$  M HCl + 0.1 M KCl solution. Furthermore,  $2 \times 10^{-3}$  M FeCl<sub>3</sub> were added to the solution under vigorous stirring. A blue solution was gradually formed, and the mixture was left to react overnight. To prepare SPG-PB active ink, the solution of

nanoparticles was used to dilute the chitosan to 1% w/v and mixed with graphite powder and glycerol as previously described. SPG-PB electrodes were prepared by using the aforementioned stencil-printing method. Finally, 5 μL of LOx and GOx were drop-cast onto the electrode surface and let to dry in ambient conditions to obtain LOx/SPG-PB and GOx/SPG-PB, respectively. The electrodes were further condition conditioned overnight in  $10 \times 10^{-3}$  M HEPES buffer pH 7.2 at +4 °C.

**Second-Generation LOx and GOx Electrode Preparation:** To prepare LOx/SPG-[Os(bpy)<sub>2</sub>(Cl)(PVI)<sub>10</sub>] and GOx/SPG-[Os(bpy)<sub>2</sub>(Cl)(PVI)<sub>10</sub>], 5 μL of ORP (1 mg mL<sup>-1</sup> in MilliQ H<sub>2</sub>O) were drop-cast onto SPG electrodes and let to dry at room temperature for 1h. Later, 5 μL of LOx and GOx were physisorbed independently onto the ORP modified electrode surface. The electrodes were further conditioned overnight in  $10 \times 10^{-3}$  M HEPES buffer pH 7.2 at +4 °C.

**Equipment and Measurements:** Cyclic voltammetry and amperometry experiments were performed using a PalmSens4 electrochemical workstation equipped with PSTrace 5.6v software. All potentials were measured using a BASi Ag|AgCl|KCl, 3 M (all potential values reported in the paper need to be considered toward this reference) and a platinum wire as reference and counter electrode, respectively. Stencil-printed graphite (SPG) electrodes (geometric area = 9 mm<sup>2</sup>, square shape  $1 \times 13 \times 3$  mm) were used as working electrodes. DRP-C110 screen-printed electrodes were used as working electrodes only for benchmarking purposes.

The morphological characterization was performed by a field emission scanning electron microscope (FE-SEM), mod. Sigma Zeiss (Jena, Germany). The images have been acquired using the in-lens detector, 5 kV acceleration voltage, 4 mm working distance, 30 μm aperture., in top-view, without any further sample treatment.

Micro-probe Raman back-scattering experiments were measured at 532 nm laser excitation wavelengths, using an NT-MDT NTEGRA system. A 50x microscope objective was used to focus the incident laser beams to a spot with a diameter of  $\approx 1 \mu\text{m}$ .

X-ray photoelectron spectroscopy analyses were carried out with Versa Probe II Scanning XPS (Physical Electronics GmbH) spectrometer equipped with Al Kα source, spot size 200 μm. Wide-scan and high-resolution spectra were obtained in CAE mode with pass energy of 117.40 and 29.35 eV, respectively, and with source power of 49.2 W. The charge compensation was performed with an electron gun operating at 1.0 V and 20.0 μA. The data were analyzed with the MultiPak v. 9.9.0.8 software.

**Volunteer for Experiments in Sweat:** A 30 years old, apparently healthy, male volunteer was participating in all measurements and procedures herein described without any minimal health risks, and written informed consent was received. The treatment of personal data was done in accordance with the provisions of the GDPR law 675/1996, based on Directive 95/46/EC, which aims to prevent the violation of personal integrity in the processing of personal data. There is no possibility of harm arising as a result of the conduct of the research project or when the information being collected is available from the public domain.

## Supporting Information

Supporting Information is available from the Wiley Online Library or from the author.

## Acknowledgements

The following funding agencies are acknowledged: Academy of Finland projects #316881, #316883 "Spatiotemporal control of Cell Functions," #332106 "ProSiT—Protein Detection at the Single-Molecule Limit with a Self-powered Organic Transistor for HIV early diagnosis"; Biosensori analitici usa-e getta a base di transistori organici auto-alimentati per la rivelazione di biomarcatori proteomici alla singola molecola per la diagnostica decentrata dell'HIV (6CDD3786); Research for Innovation REFIN—Regione Puglia POR PUGLIA FESR-FSE 2014/2020; PMGB ARS01\_01195; NoOne-A binary sensor with single-molecule digit to discriminate biofluids enclosing zero or at least one biomarker, ERC Stg2021, GA:101040383;



PRIN project prot.2017RHX2E4 "At the forefront of Analytical ChemisTry: dirUptive detection technoLogies to improve food safety—ACTUaL"; IDF SHARID (ARS01\_01270); Abo Akademi University CoE "Bioelectronic activation of cell functions"; University of Galway College of Science and Engineering Scholarship and CSGI are acknowledged for partial financial support.

## Conflict of Interest

The authors declare no conflict of interest.

## Author Contributions

A.T. and A.I. contributed equally to this work. P.B. conceived the project and wrote the manuscript. A.T., A.I. and M.V., performed all electrochemical measurements. N.D. performed XPS analyses. C.D.F. performed SEM measurements. M.P. and G.S. performed Raman spectroscopy measurements. R.K. synthesized the osmium redox polymers. D.L. supervised R.K. G.P. kindly provided lactate oxidase. P.B. and E.M. directly supervised A.T., A.I., and M.V. during the project. D.L., L.T., G.S., E.M., and P.B. revised the manuscript. The final version was approved by all authors.

## Data Availability Statement

The data that support the findings of this study are available from the corresponding author upon reasonable request.

## Keywords

glucose biosensors, lactate biosensors, modified electrodes, water-based conductive inks, wearable biosensors

Received: February 28, 2023  
Revised: April 5, 2023  
Published online: April 25, 2023

- [1] P. Bollella, *Anal. Chim. Acta* **2022**, *1234*, 340517.  
[2] J. Kim, A. S. Campbell, B. E.-F. de Ávila, J. Wang, *Nat. Biotechnol.* **2019**, *37*, 389.  
[3] J. Wang, *Chem. Rev.* **2008**, *108*, 814.  
[4] E. Battista, V. Lettera, M. Villani, D. Calestani, F. Gentile, P. A. Netti, S. Iannotta, A. Zappettini, N. Coppede, *Org. Electron.* **2017**, *40*, 51.  
[5] P. Bollella, *Nanomaterials* **2020**, *10*, 722.  
[6] R. Shiwaku, H. Matsui, K. Nagamine, M. Uematsu, T. Mano, Y. Maruyama, A. Nomura, K. Tsuchiya, K. Hayasaka, Y. Takeda, *Sci. Rep.* **2018**, *8*, 3922.  
[7] E. Sardini, M. Serpelloni, S. Tonello, *Biosensors* **2020**, *10*, 166.  
[8] M. Elbadawi, J. J. Ong, T. D. Pollard, S. Gaisford, A. W. Basit, *Adv. Funct. Mater.* **2021**, *31*, 2006407.  
[9] J. Wang, M. Musameh, *Analyst* **2004**, *129*, 1.  
[10] Bolon: UV Radiation curable electrically conductive... – Google Scholar, [https://scholar.google.com/scholar\\_lookup?title=UV%20Radiation%20Curable%20Electrically%20Conductive%20Ink%20and%20Circuit%20Boards%20Made%20Therewith&publication\\_year=1978&author=D.A.%20Bolon&author=G.M.%20Lucas&author=S.H.%20Schroeter,n.d.\(accessed:February2023\).](https://scholar.google.com/scholar_lookup?title=UV%20Radiation%20Curable%20Electrically%20Conductive%20Ink%20and%20Circuit%20Boards%20Made%20Therewith&publication_year=1978&author=D.A.%20Bolon&author=G.M.%20Lucas&author=S.H.%20Schroeter,n.d.(accessed:February2023).)  
[11] E. Dimitriou, N. Michailidis, *Nanotechnology* **2021**, *32*, 502009.  
[12] J. R. Camargo, L. O. Orzari, D. A. G. Araujo, P. R. de Oliveira, C. Kalinke, D. P. Rocha, A. L. dos Santos, R. M. Takeuchi, R. A. A. Munoz, J. A. Bonacin, *Microchem. J.* **2021**, *164*, 105998.

- [13] H. P. Kn, C. S. Meghana, N. K. Raju, S. P. Shilpa, M. R. Yashaswini, C. Manjunatha, *ECS Trans.* **2022**, *107*, 11261.  
[14] A. Gevaerd, E. Y. Watanabe, C. Belli, L. H. Marcolino-Junior, M. F. Bergamini, *Sens. Actuators, B* **2021**, *332*, 129532.  
[15] D. A. Araujo, J. R. Camargo, L. A. Pradela-Filho, A. P. Lima, R. A. Munoz, R. M. Takeuchi, B. C. Janegitz, A. L. Santos, *Microchem. J.* **2020**, *158*, 105297.  
[16] J. R. Camargo, T. A. Silva, G. A. Rivas, B. C. Janegitz, *Electrochim. Acta* **2022**, *409*, 139968.  
[17] Y. Aleeva, B. Pignataro, *J. Mater. Chem. C* **2014**, *2*, 6436.  
[18] N. Hasegawa, A. Kamiya, T. Matsunaga, N. Kitano, M. Harada, *Colloids Surf. A* **2021**, *628*, 127153.  
[19] Y. Bonnassieux, C. J. Brabec, Y. Cao, T. B. Carmichael, M. L. Chabynec, K.-T. Cheng, G. Cho, A. Chung, C. L. Cobb, A. Distler, *Flexible Printed Electron.* **2021**, *6*, 023001.  
[20] J. R. Sempionatto, V. R.-V. Montiel, E. Vargas, H. Teymourian, J. Wang, *ACS Sens.* **2021**, *6*, 1745.  
[21] J. R. Sempionatto, J. A. Lasalde-Ramírez, K. Mahato, J. Wang, W. Gao, *Nat. Rev. Chem.* **2022**, *6*, 8991.  
[22] J. Min, J. R. Sempionatto, H. Teymourian, J. Wang, W. Gao, *Biosens. Bioelectron.* **2021**, *172*, 112750.  
[23] K. Van Hoovels, X. Xuan, M. Cuartero, M. Gijssels, M. Swarén, G. A. Crespo, *ACS Sens.* **2021**, *6*, 3496.  
[24] J. Ye, T. Chu, J. Chu, B. Gao, B. He, *ACS Sustainable Chem. Eng.* **2019**, *7*, 18048.  
[25] B. Schmiege, J. Döbber, F. Kirschhöfer, M. Pohl, M. Franzreb, *Front. Bioeng. Biotechnol.* **2019**, *6*, 211.  
[26] E. G. Michael, *Analyst* **1996**, *121*, 715.  
[27] P. Bollella, L. Gorton, *Curr. Opin. Electrochem.* **2018**, *10*, 157.  
[28] P. Bollella, E. Katz, *Sensors* **2020**, *20*, 3517.  
[29] T. Adachi, Y. Kitazumi, O. Shirai, K. Kano, *Catalysts* **2020**, *10*, 236.  
[30] F. Lisdat, *Biosensing for the 21st Century*, Springer, Berlin **2007**.  
[31] F. Lisdat, *Bioelectrochemistry* **2020**, *134*, 107496.  
[32] L. Gorton, *Special Issue on Sugar Oxidising Enzymes*, Elsevier, Amsterdam **2020**.  
[33] I. Leiros, E. Wang, T. Rasmussen, E. Oksanen, H. Repo, S. B. Petersen, P. Heikinheimo, E. Hough, *Acta Crystallogr. Sect. F: Struct. Biol. Cryst. Commun.* **2006**, *62*, 1185.  
[34] E. N. Biryukova, A. Y. Arinbasarova, A. G. Medentsev, *Microbiology* **2022**, *91*, 124.  
[35] S. B. Bankar, M. V. Bule, R. S. Singhal, L. Ananthanarayan, *Biotechnol. Adv.* **2009**, *27*, 489.  
[36] P. N. Bartlett, F. A. Al-Lolage, *J. Electroanal. Chem.* **2018**, *819*, 26.  
[37] G. S. Wilson, *Native Glucose Oxidase Does Not Undergo Direct Electron Transfer*, Biosensors and Bioelectronics, Elsevier Ltd. **2016**.  
[38] F. Li, J. Liu, L. Guo, J. Wang, K. Zhang, J. He, H. Cui, *Biosens. Bioelectron.* **2019**, *141*, 111472.  
[39] R. Rathod, B. Gajera, K. Nazir, J. Wallenius, V. Velagapudi, *Metabolites* **2020**, *10*, 103.  
[40] E. H. Suh, C. F. Galdes, S. Chirayil, B. Faubert, R. Ayala, R. J. DeBerardinis, A. D. Sherry, *Cancer Metabolism* **2021**, *9*, 38.  
[41] T. R. Paixão, *ChemElectroChem* **2020**, *7*, 3414.  
[42] I. Lavagnini, R. Antiochia, F. Magno, *Electroanalysis* **2004**, *16*, 505.  
[43] A. C. Ferrari, J. C. Meyer, V. Scardaci, C. Casiraghi, M. Lazzeri, F. Mauri, S. Piscanec, D. Jiang, K. S. Novoselov, S. Roth, A. K. Geim, *Phys. Rev. Lett.* **2006**, *97*, 187401.  
[44] A. C. Ferrari, *Solid State Commun.* **2007**, *143*, 47.  
[45] F. Tuinstra, J. L. Koenig, *J. Chem. Phys.* **2003**, *53*, 1126.  
[46] A. A. Karyakin, O. V. Gitelmacher, E. E. Karyakina, *Anal. Chem.* **1995**, *67*, 2419.  
[47] A. Ramanavicius, A. I. Rekertaitė, R. Valiūnas, A. Valiūnienė, *Sens. Actuators, B* **2017**, *240*, 220.  
[48] M. A. Komkova, E. E. Karyakina, A. A. Karyakin, *J. Am. Chem. Soc.* **2018**, *140*, 11302.

- [49] S. Cinti, R. Cusenza, D. Moscone, F. Arduini, *Talanta* **2018**, *187*, 59.
- [50] A. A. Karyakin, *Electroanalysis* **2001**, *13*, 813.
- [51] P. Xu, T. Yano, K. Yamamoto, H. Suzuki, H. Kumagai, *Appl. Biochem. Biotechnol.* **1996**, *56*, 277.
- [52] M. A. Zia, K.-U. Rahman, M. K. Saeed, F. Andaleeb, M. I. Rajoka, M. A. Sheikh, I. A. Khan, A. I. Khan, *J. Clin. Biochem. Nutr.* **2007**, *41*, 132.
- [53] S. Pérez, E. Fàbregas, *Analyst* **2012**, *137*, 3854.
- [54] L. V. Shkotova, T. B. Goriushkina, C. Tran-Minh, J.-M. Chovelon, A. P. Soldatkin, S. V. Dzyadevych, *Mater. Sci. Eng., C* **2008**, *28*, 943.
- [55] E. I. Yashina, A. V. Borisova, E. E. Karyakina, O. I. Shchegolikhina, M. Y. Vagin, D. A. Sakharov, A. G. Tonevitsky, A. A. Karyakin, *Anal. Chem.* **2010**, *82*, 1601.
- [56] A. Sannini, D. Albanese, F. Malvano, A. Crescitelli, M. Di Matteo, *Chem. Eng. Trans.* **2015**, *44*, 283.
- [57] L. C. Korneyeva, A. V. Borisova, Y. I. Yashina, E. E. Karyakina, O. G. Voronin, S. Cosnier, A. A. Karyakin, *Moscow Univ. Chem. Bull. (Engl. Transl.)* **2010**, *65*, 49.
- [58] S. A. Marzouk, H. E. Sayour, A. M. Ragab, W. E. Cascio, S. S. Hassan, *Electroanalysis* **2000**, *12*, 1304.
- [59] B. Alp, S. Mutlu, M. Mutlu, *Food Res. Int.* **2000**, *33*, 107.
- [60] I. L. de Mattos, M. C. da Cunha Areias, *Talanta* **2005**, *66*, 1281.
- [61] A. Popov, R. Aukstojyte, J. Gaidukevic, V. Lisyte, A. Kausaite-Minkstimiene, J. Barkauskas, A. Ramanaviciene, *Sensors* **2021**, *21*, 948.
- [62] A. Kausaite-Minkstimiene, L. Glumbokaite, A. Ramanaviciene, A. Ramanavicius, *Microchem. J.* **2020**, *154*, 104665.
- [63] M. Artigues, J. Abellà, S. Colominas, *Sensors* **2017**, *17*, 2620.
- [64] N. C. Sekar, S. A. M. Shaegh, S. H. Ng, L. Ge, S. N. Tan, *Sens. Actuators, B* **2014**, *204*, 414.
- [65] R. Bennett, E. Blochouse, D. Leech, *Electrochim. Acta* **2019**, *302*, 270.
- [66] W. Gao, S. Emaminejad, H. Y. Y. Nyein, S. Challa, K. Chen, A. Peck, H. M. Fahad, H. Ota, H. Shiraki, D. Kiriya, D.-H. Lien, G. A. Brooks, R. W. Davis, A. Javey, *Nature* **2016**, *529*, 509.
- [67] P. S. Petrou, I. Moser, G. Jobst, *Biosens. Bioelectron.* **2003**, *18*, 613.
- [68] A. F. Revzin, K. Sirkar, A. Simonian, M. V. Pishko, *Sens. Actuators, B* **2002**, *81*, 359.
- [69] P. Bollella, S. Sharma, A. E. G. Cass, R. Antiochia, *Electroanalysis* **2019**, *31*, 374.
- [70] K. Jayakumar, R. Bennett, D. Leech, *Electrochim. Acta* **2021**, *371*, 137845.
- [71] H. Chen, Y. Ma, X. Wang, X. Wu, Z. Zha, *RSC Adv.* **2017**, *7*, 248.